Analysis of the Optical Coupling Between GaSb Diode Lasers and Passive Waveguides: A Step Toward Monolithic Integration on Si Platforms

Michele Paparella, Laura Monge Bartolome, Jean-Baptiste Rodriguez, Laurent Cerutti, Marco Grande, Liam Oafaolain, Eric Tournie

Analysis of the Optical Coupling Between GaSb Diode Lasers and Passive Waveguides: A Step Toward Monolithic Integration on Si Platforms

Michele Paparella, Laura Monge Bartolome, Jean-Baptiste Rodriguez, Laurent Cerutti, Marco Grande, Liam O'Faolain, and Eric Tournié

***Abstract*—We simulate the optical coupling between 2.3 μm GaSb-based diode lasers (DLs) epitaxially grown on on-axis silicon (001) and passive waveguides in the butt-coupling geometry. 3D FDTD simulations reveal how the optical coupling is affected by the air gap between the laser cavity and the waveguide that arises from the laser etched-facet definition. We also model alternative approaches consisting in filling the gap with higher-refractive index materials transparent in the mid-infrared window. Finally, because of their fabrication flexibility, we propose to implement polymeric waveguides in order to achieve improved coupling performances.**

***Index Terms*—III-V integration on Si, photonic integrated circuits, silicon photonics.**

I. Introduction

Nowadays, Silicon photonics is a very important technology in order to realize optical interconnects with reduced energy consumption [1]. Although Si photonics has been very successful particularly for telecom applications, the miniaturization provided by Photonic Integrated Circuits (PICs) can also be implemented for environmental sensing, agri-food analysis, industrial processing monitoring with particular focus on gas detection and biomedical sensing [2], [3], [4], [5]. The Mid-Infrared (MIR) wavelength window shows fingerprint absorption lines for many different species. Particularly, gases such as $\mathbf{CH_4}$, $\mathbf{NH_3}$ or CO absorb in the wavelength range of 2–2.5 $\mu\mathbf{m}$ with $\mathbf{CH_4}$ displaying its second most important absorption line at $\sim$2.3 $\mu\mathbf{m}$ [6]. The driving forces behind the increased use of silicon PICs are based on the following points: i) availability of cheap Si wafers and well developed process technology, ii) strong optical confinement due to the high index contrast between Si and $\mathbf{SiO_2}$ in Silicon-on-Insulator (SOI) platforms, iii) high thermal conductivity, optical damage threshold and third-order nonlinearities, iv) low-losses in the wavelength range between 1.1 and $\sim 6.5\ \mu\mathbf{m}$, depending on the material used [7]. Among those, Silicon Nitride (SiN) photonics is an emerging platform, opening new paths for realization of photonic devices with improved performances. SiN shows transparency also for visible wavelengths unlike Si, still providing high-index contrast and compatibility with CMOS fabrication, reduction of spurious reflections, manufacturing flexibility, improved losses properties and small sensitivity to changes in temperature [8], [9]. Nowadays, this platform is used to realize low-loss waveguides [10], grating waveguides [11] and high Q-factor micro resonators [12], [13], [14].

However, both Si and SiN with $\mathbf{SiO_2}$ cladding layer waveguides cannot operate properly above wavelengths of $\sim 3.5\ \mu\mathbf{m}$ for $\mathbf{SiO_2}$ starts to absorb [15], [16].

Nevertheless, the main silicon photonics' bottleneck is related to its indirect bandgap making it a very inefficient light emitter.

Despite different efforts to realize Germanium (Ge) based lasers [17], [18], III-V semiconductor laser diodes (LDs) remain until now the best technology to get coherent light emission and the only suitable light sources for PICs. The most mature approach to combine light sources with passive optical devices is based on heterogeneous integration [19], [20], [21], [22]. The integration of the active devices is achieved by means of bonding procedures such as direct, molecular, or polymer bonding [23], or micro-transfer printing ($\boldsymbol{\mu TP}$) [24], [25]. The use of native III-V substrates results in high structural quality and optimal laser performances. On the other hand, III-V substrates are small and expensive and are wasted in these integration schemes. Also, an accurate alignment is required when the III-V sample is transferred onto the Si platform. For these reasons, in this work we consider another approach where the III-V laser heterostructure is directly grown on the Si PIC before being processed to form the laser source [23]. Exploiting this

Manuscript received 13 June 2022; revised 30 July 2022; accepted 28 August 2022. Date of publication 1 September 2022; date of current version 14 September 2022. This work was supported in part by the Horizon 2020 Program of the European Union through REDFINCH under Grants GA 780240 and through OPTAPHI under Grant GA 860808, and in part by the French Program on Investments for the Future through EXTRA under Grant ANR-11-EQPX-0016. *(Corresponding author: Michele Paparella.)*

Michele Paparella is with the IES, CNRS, University of Montpellier, F-34000 Montpellier, France, and also with the Department of Electrical and Information Engineering, Polytechnic University of Bari, IT-70126 Bari, Italy (e-mail: michele.paparella@umontpellier.fr).

Laura Monge Bartolome, Jean-Baptiste Rodriguez, Laurent Cerutti, and Eric Tournié are with the IES, CNRS, University of Montpellier, F-34000 Montpellier, France (e-mail: laura.monge-bartolome@umontpellier.fr; jean-baptiste.rodriguez@cnrs.fr; laurent.cerutti@umontpellier.fr; eric.tournie@umontpellier.fr).

Marco Grande is with the Polytechnic University of Bari, IT-70126 Bari, Italy (e-mail: marco.grande@poliba.it).

Liam O'Faolain is with the Centre for Advanced Photonics and Process Analysis, Munster Technological University, IR-T12P928 Cork, Ireland, and also with Tyndall National Institute, IR-T12R5CP Cork, Ireland (e-mail: william.whelan-curtin@mtu.ie).

Digital Object Identifier 10.1109/JPHOT.2022.3203593

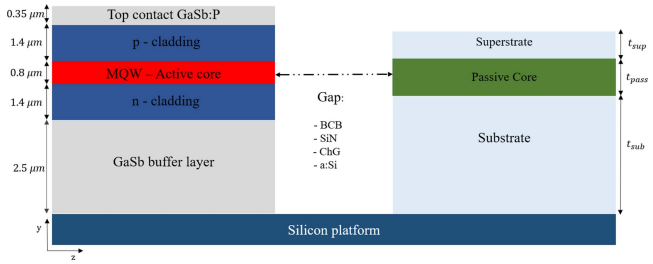

Fig. 1. 2D cross section of the laser and passive waveguide layer stack. The details concerning the geometrical parameters and the filling gap materials are reported in Table I.

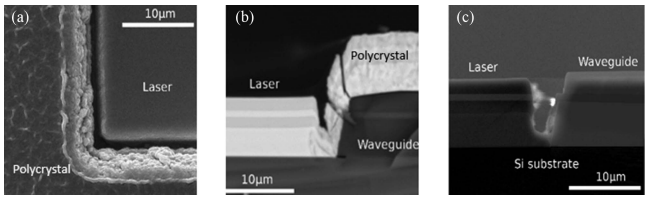

Fig. 2. Scanning Electron Microscope images of a GaSb DL grown on a Si substrate supporting SiN/SiO_2 waveguides. (a) Plan view of the interface between the laser structure and the waveguide right after epitaxial growth, (b) cross section view of the same area, and (c) cross-section view after polycrystal removal.

integration technique, we study the optical transmission in a butt coupled geometry as depicted in Fig. 1. In more details, we consider a GaSb-DL grown on on-axis (001) Si substrates by Molecular Beam Epitaxy (MBE).

The laser heterostructure is made of two GaInAsSb quantum wells (QWs), an $Al_{0.25}Ga_{0.75}As_{0.02}Sb_{0.98}$ waveguide with bottom and top claddings made of $Al_{0.9}Ga_{0.1}As_{0.07}Sb_{0.93}$.

Note that growing the laser structure after waveguide definition allows for an accurate alignment of the laser active zone with the waveguide (Fig. 2(c)). For more details about the growth procedure and laser performances, the reader is referred to [26].

In this approach, the cavity mirrors cannot be fabricated by cleaving anymore. An alternative approach suitable for on-chip applications is based on the definition of etched-cavity ridge DLs, where both the ridge and the mirror facets are defined by using UV photolithography and inductively-coupled plasma reactive ion etching (ICP-RIE) [27]. However, during epitaxy of the III-V laser on a Si wafer supporting SiN/SiO_2 waveguides poor quality III-V materials are deposited close to the passive waveguide interface and should be removed, which invariably results in an air gap separating the passive and active waveguides (Fig. 2(c)). Moreover, the SEM pictures show that we can achieve a gap 5 μm wide.

In this article, we first study the optical coupling between a GaSb-based DL and a passive waveguide made of SiN, Si, Germanium (Ge) and Chalcogenide (ChG). 3D Finite Difference Time Domain (FDTD) simulations are performed to evaluate the transmitted power as function of the air gap between the active and passive sections. They show a high light coupling in the absence of a gap between the two waveguides. However, the introduction of an unavoidable air gap drastically reduces the optical transmission. In order to improve the coupling performances, we also propose alternative approaches such as filling the gap with high refractive index materials or using polymer-based optical waveguides.

II. FDTD Simulation Results

A. Finite Difference Time Domain Simulations

The optical coupling behavior has been modeled with a Finite Difference Time Domain (FDTD) numerical approach. FDTD provides a solution of the Maxwell's equation both in the spatial and time domain, proving to be a more robust method for devices with variations in the order of light wavelength and energy flow in random directions [28], as in our case study where the presence of the beam divergence cannot be neglected.

The computational space is divided into discrete points as well as time in discrete steps. The input source is shaped as a Continuous Wave (CW) - Gaussian beam profile with a driving wavelength $\lambda = 2.3\ \mu m$ and it propagates from the active into the passive waveguide. The optical mode is settled to be TE-polarized with the electric field component lying along the x-axis. When the optical device is properly excited, both the electric and magnetic fields are computed for each discrete space points and time steps. The choice of finer space points and time steps will provide an approximation not far from the continuous equations [29]. However, FDTD requires a not negligible computational effort with powerful machine resources. We simulate the optical coupling of the hybrid device based on a 3D FDTD model. The grid is defined as 20 Point Per Wavelength (PPW) in the material of the waveguide with a corresponded spatial uniform grid size ($\Delta x,\ \Delta y,\ \Delta z$) of 30 nm. This grid size values ensure the Courant condition needed for the simulation stability. In the model, we set the Courant number to 0.95. Both the active and passive waveguides have been modeled as buried channel with a customized refractive index for each layer. A monitor is settled to collect the amount of power coupled into the passive waveguide and it is located before the end of the waveguide.

B. Waveguide Based on Silicon Technology

In this section, we focus on the light transmission analysis based on a butt-coupled geometry between a GaSb - LD and a passive waveguide. A similar approach has been exploited for coupling light into a SiN based waveguide, though with a Superluminescent LED (SLED) as light source [30]. In our work, we firstly analyze the coupling performances with a SiN passive core before moving to different passive core materials such as Si, Ge and ChG. Then, we show alternative opportunities for coupling improvement based on the use of high-index materials in order to avoid air in the gap. Furthermore, we investigate a possible benefit that can arise from introducing a thick SiN layer in our model.

In more details, we use the gain section made of an active waveguide ($n_{a,\ core} = 3.695$) and surrounded by a top and bottom cladding ($n_{a,\ cladd} = 3.27$). This section is butt coupled with the passive device. The LD ridge as well as the passive waveguide is chosen to be 10 μm wide. For the optical coupling modeling, we assume a lossless media and an

TABLE I
GEOMETRICAL DETAILS AND REFRACTIVE INDICES OF THE FILLING MATERIALS EMPLOYED IN THE 3D MODEL

Thickness	Value
p-cladding	1.4 μm
Active core	0.83 μm
n-cladding	1.4 μm
Superstrate	1 μm
Passive core	0.8-2.6 μm
Substrate	3.8 μm
Filling materials	**Refractive index**
Air	1
BCB	1.53
SiN	2.01
ChG ($Al_{20}Se_{80}$)	2.59
a:Si	3.44

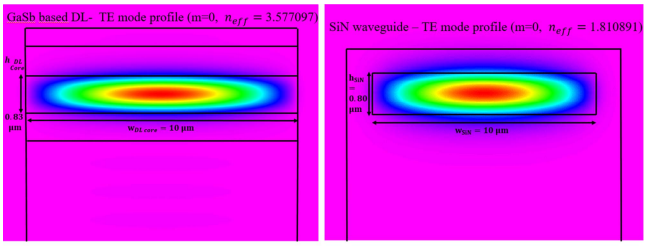

(a)

Fig. 3. 2D TE mode profile related to 10 μm wide (a) DL ridge (b) SiN waveguide.

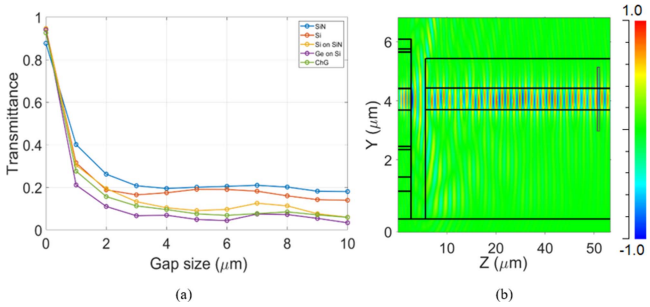

(a) (b)

Fig. 4. (a) Transmittance as a function of air gap sizes for different passive core materials. (b) Counter map of the electric field profile related to the fundamental TE optical mode for an air gap 3 μm wide and monitor located before the end of the end of the passive waveguide ($\sim 55\ \boldsymbol{\mu m}$).

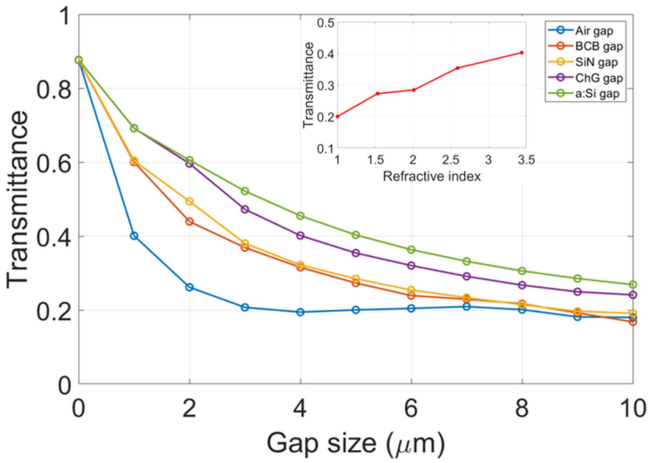

Fig. 5. Coupling study for a SiN waveguide: (a) Transmittance as a function of gap sizes filled with different materials. The inset also outlines a transmittance improvement as the refractive index value, in a gap 5 μm wide, is increased.

emission wavelength fixed at $\lambda = 2.3\ \mu$m. The geometrical details associated to the different layer thicknesses and the filling gap materials are reported in Table I.

Firstly, we analyze the impact of the air gap on the light coupling for a SiN ($n_{SiN} = 2$) waveguide surrounded by a SiO_2 ($n_{SiO_2} = 1.44$) cladding. It is worth pointing out that the gap cannot be avoided. For this reason, it is crucial to study how the air distance between the optical devices will affect the coupling. The same study is made for different core materials ($n_{Si} = 3.44$, $n_{Ge} = 4$, $n_{ChG} = 2.59$) as plotted in Fig. 4(a).

A mode overlap study has been carried out before investigating the air gap effect on the optical coupling, proving that choosing both DL ridge as well as a SiN waveguide 10 μm wide provides an overlap value $\sim 86\%$. The 2D mode profiles supported by the DL ridge and SiN waveguide are plotted in Fig. 3.

The fundamental TE mode propagates from the active region (left) into the SiN waveguide (right) as shown in Fig. 4(b). As expected, the optical mode is not confined, and the light beam undergoes a divergence as it propagates in the free space.

The simulation results point out a remarkable coupling reduction when the air gap is introduced. Particularly, the transmittance decreases from $\sim$ 80% down to $\sim$ 20% for a 5 μm gap width, and it stays approximately constant for wider gaps. This is most likely due to a Fabry-Perot (FP) interferometer effect where the two parallel mirrors consist of passive and active core layer end-facets with air in the middle. Even when using other materials for the passive core, the transmittance is enhanced only if there is no separation between the sections of the hybrid device. This last aspect can be seen when materials with a higher refractive index compared to SiN (e.g., Si, Ge or ChG) are introduced. In this case, the index contrast between active and passive layer is decreased, while the transmittance is improved. However, as the air gap width increases, the coupling behavior shows the same decay trend. These results outline the strong influence due to the presence of the air gap and the necessity to reduce it in order to achieve improved coupling performances.

However, filling the gap with higher refractive index materials, should reduce the beam divergence and improve the coupling. We now investigate this approach.

Materials such as Benzocyclobutene (BCB), SiN [31], ChG [32] and amorphous Silicon (a:Si) [33] have been chosen for our study since they are transparent in the MIR wavelength range.

The results plotted in Fig. 5 show enhanced coupling when the gap is filled with high - index materials. In more details, the inset in Fig. 5 plots the transmittance as a function of the

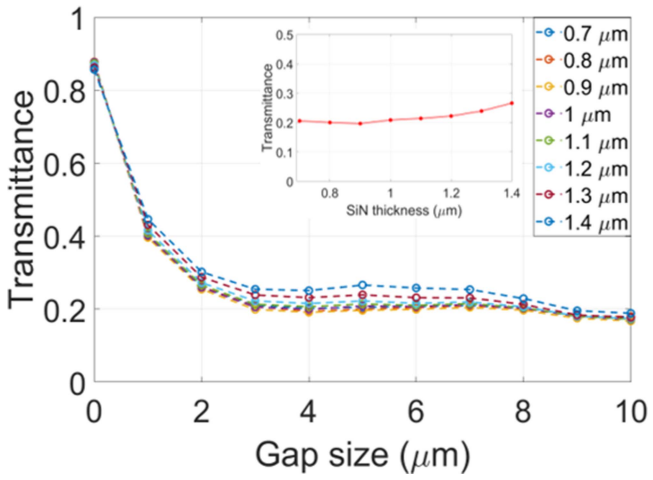

Fig. 6. Study of the influence of SiN layer thickness (0.7–1.4 μm) on the optical coupling as function of different gap sizes. The inset shows an improvement of ∼10% when the SiN layer is 1.4 μm thick for a fixed air gap 5 μm wide.

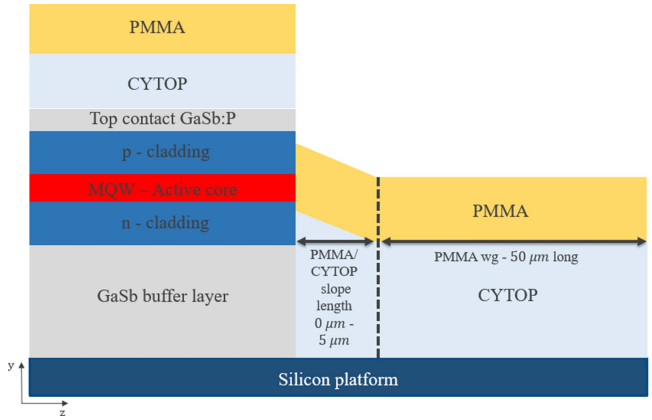

Fig. 7. Hybrid configuration with a passive layers stack based on polymer materials.

different refractive indices used for filling the gap. In this case, considering a 5-µm wide gap, the results show a doubling in optical coupling from $\sim 20\%$ (air gap) to $\sim 40\%$ (a-Si gap). These results show that this approach is promising to overcome the air gap influence on the light transmission. Among the different materials investigated, a-Si is the most efficient. However, filling the gap with a-Si would not be easy to implement as it would require deposition of a thick conformal a-Si layer. Moreover, due to a higher a-Si refractive index, it can reduce the laser facet reflection and thus deteriorate the device performances, although one could get around this potential issue by depositing a high-reflectivity coating on the opposite facet. Finally, a-Si could also create shorts on the laser facets. An alternative, viable approach is to use BCB, that can be deposited by spin coating and should easily fill the gap. The optical coupling enhancement however will be smaller than with the other filling materials listed in Table I.

A further approach for the coupling optimization has been investigated where the influence of the SiN thickness has been evaluated. As shown in Fig. 6, we study the transmittance for thicker SiN core layer as function of the air gap size. Particularly, considering the air gap 5 μm wide and taking into account a thicker SiN layer (e.g., 1.4 μm), the transmittance reaches a value close to 30% with a relative increase of $\sim 10\%$ if compared with a 0.8 μm thick SiN layer. Even if this approach could provide some benefits, we may experience difficulties due to deposition of thick SiN film which could result in cracks formation [14]. Moreover, the enhancement provided by using this approach does not show the same strength of the strategy discussed previously.

C. Polymer Waveguides

In the previous section, we identified an important challenge to overcome: enhancing the coupling either by minimizing the distance between the two optical devices or filling the gap by means of high refractive index materials. However, these solutions can prove elusive because of a lack of experimental feasibility. The idea of using polymer based waveguides arise from their flexible fabrication by using spin-coating technique and subsequently implement thermal curing procedures in order to realize optical waveguides [34], [35]. By means of this approach, the air gap is suppressed as the polymeric material will match the end facet of the laser diode thanks to a uniform distribution. In the literature, several works reported optical waveguides based on polymers for telecom applications as these materials are optically transparent in the corresponding wavelength range [25], [34], [35], [36]. However, a recent study [35] has shown that polymers exhibit absorption features in the MIR region that can affect the light transmission through them and their extinction coefficient is higher than those at telecom wavelengths.

In this section, we analyze the optical coupling for $\lambda = 2.3\ \mu m$ into a passive polymer-based waveguide. We consider a cyclised transparent optical polymer (CYTOP) lower cladding ($n_{CYTOP} = 1.34$) with a Polymethyl methacrylate (PMMA, $n_{PMMA} = 1.47$) core and an air top cladding and at the sidewalls (Fig. 6). Firstly, we evaluate the transmitted power considering a lossless PMMA material. After, we introduce the extinction coefficients 5×10^{-3} and 1×10^{-3} analyzed in the two model reported [37]. The difference in values can be attributed to the uncertainty of industrial process and injection parameters as explained by the authors in [37]. For this configuration, we need to point out some requirements needed to allow a correct optical mode propagation.

First, preliminary simulations outline the importance of setting the cladding thickness larger than 2 μm in order to avoid optical mode leakage into the Si substrate. For this reason, we choose a bottom cladding thickness of 3 μm. However, by varying the cladding thickness we change the passive core alignment with the active zone. It is important to avoid longitudinal misalignment in order to effectively collect light. Here, we take into account a hybrid device based on a polymeric waveguide properly aligned with the active region (Fig. 7). Also, a 2.6 μm thick PMMA core is chosen such that the optical mode is properly confined into the waveguide. In fact, for a PMMA

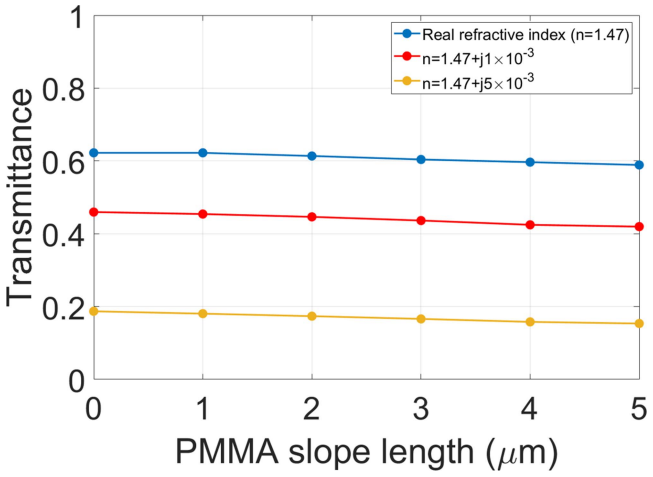

Fig. 8. Transmittance as function of the PMMA slope length.

thickness less than $2\ \mu$m, the effective refractive index of the optical mode is roughly 1.37 close to the one of CYTOP. For this reason, the mode is pushed toward the cladding instead to be properly confined in the core. Moreover, we expect a sloped configuration - due to the polymer spinning process -before reaching a planar waveguide configuration as shown in Fig. 7.

The optical coupling as function of the PMMA slope width is shown in Fig. 8. The plot outlines the transmittance taking into account the PMMA real refractive index and PMMA complex refractive index based on two different models [37].

When we consider the PMMA planar waveguide, the light transmission into the polymer waveguide is $\sim 60\%$, that is smaller than the $\sim 80\%$ in the case of SiN waveguide as previously discussed, due to the lower refractive index of PMMA. For this reason, reflections are stronger due to a higher refractive index contrast at the end-facet interface between the DL and the PMMA waveguide which induces a decrease of the light transmission. However, due to the polymer spinning and the presence of the DL that can essentially acts as an obstacle for the uniform distribution of the material, it is reasonable to consider a PMMA slope configuration before reaching a planar waveguide geometry. Based on typical resist spinning process, we assume that the slope can be up to $5\ \mu$m long and we investigate how this geometry can affect the optical coupling.

As plotted in Fig. 8, the transmittance stays almost constant even with the assumption of a sloped configuration. From these results, this polymer waveguide configuration shows an important optical coupling stability. It also represents a valid alternative approach in order to avoid any air gap that could affect the optical coupling as previously discussed. However, the coupling performances can deteriorate when the imaginary part of the PMMA complex refractive index is taken into account [37]. In more details, with an extinction coefficient of 1×10^{-3}, the transmitted power into the PMMA waveguide reaches values close to 40%, which is equivalent to the scenario where a-Si is used as filling material in the gap. The worst scenario is shown when the extinction coefficient reaches a value of 5×10^{-3}. Even when using waveguide with a small refractive index contrast, this configuration looks a promising way to optimize the light transmission with a butt coupled geometry. Moreover, once established a reasonable light coupling enhancement exploiting the approach based on polymer waveguides, these last could be used as a bridge toward PICs on silicon waveguide [38], [39].

III. Conclusion

We have simulated the optical coupling between $2.3\ \mu$m GaSb-based laser diodes (LDs) epitaxially grown on-axis silicon (001) and on chip passive waveguides. The hybrid device proposed exploits a butt-coupling geometry. The definition of the laser facets through etching introduces an air gap that reduce drastically the optical transmittance from more than 80% down to 20% for a $5\ \mu m$ wide air gap. Different possible solutions for the coupling optimization have been analyzed and one of the most promising approaches consists in filling the gap with higher refractive index materials, such as a-Si with a remarkable transmittance enhancement. However, among all these gap filling materials, only BCB could be easily experimentally managed. On the other hand, polymer based optical waveguides are widely used at telecom wavelengths because of their rapid processability and cost effectiveness as well as high optical transparency. However, close to the MIR region, polymers start to be less transparent compared to shorter wavelengths. By taking into account the complex refractive index as function of wavelengths, simulation results show stable performances even if with lower transmittance values. However, the instability of the imaginary part related to the PMMA complex refractive index can affect the light coupling. Nevertheless, polymer waveguides are attractive as an "optical bridge" to transfer the optical mode from the polymer into a tapered SiN waveguide by exploiting a vertical coupling. In future work we will fabricate and characterize the hybrid device with a GaSb-based LD and SiN waveguide in order to experimentally evaluate the coupling losses due to the air gap. As next step we would like to fill the gap comparing the two transmittance behaviors (i.e., air and high index materials) and successively implement the approach based on polymeric waveguide.

References

[1] Q. Cheng, M. Bahadori, M. Glick, S. Rumley, and K. Bergman, "Recent advances in optical technologies for data centers: A review," *Optica*, vol. 5, no. 11, pp. 1354–1370, Nov. 2018, doi: 10.1364/OPTICA.5.001354.

[2] J. T. Robinson, L. Chen, and M. Lipson, "On-chip gas detection in silicon optical microcavities," in *Proc. Conf. Lasers Electro-Opt. Conf. Quantum Electron. Laser Sci.*, 2008, Art. no. 6.

[3] N. A. Yebo et al., "Selective and reversible ammonia gas detection with nanoporous film functionalized silicon photonic micro-ring resonator," *Opt. Exp.*, vol. 20, no. 11, pp. 11855–11862, May 2012, doi: 10.1364/OE.20.011855.

[4] T. H. Stievater et al., "Trace gas absorption spectroscopy using functionalized microring resonators," *Opt. Lett.*, vol. 39, no. 4, pp. 969–972, Feb. 2014, doi: 10.1364/OL.39.000969.

[5] W.-C. Lai, S. Chakravarty, Y. Zou, and R. T. Chen, "Silicon nanomembrane based photonic crystal microcavities for high sensitivity bio-sensing," *Opt. Lett.*, vol. 37, no. 7, pp. 1208–1210, Apr. 2012, doi: 10.1364/OL.37.001208.

[6] L. S. Rothman et al., "The HITRAN2012 molecular spectroscopic database," *J. Quant. Spectrosc. Radiat. Transf.*, vol. 130, pp. 4–50, Nov. 2013, doi: 10.1016/j.jqsrt.2013.07.002.

[7] B. Jalali and S. Fathpour, "Silicon photonics," *J. Lightw. Technol.*, vol. 24, no. 12, pp. 4600–4615, Dec. 2006, doi: 10.1109/JLT.2006.885782.

[8] A. Rahim et al., "Expanding the silicon photonics portfolio with silicon nitride photonic integrated circuits," *J. Lightw. Technol.*, vol. 35, no. 4, pp. 639–649, Feb. 2017, doi: 10.1109/JLT.2016.2617624.

[9] S. Iadanza et al., "Thermally stable hybrid cavity laser based on silicon nitride gratings," *Appl. Opt.*, vol. 57, no. 22, pp. E218–E223, Aug. 2018, doi: 10.1364/AO.57.00E218.

[10] D. J. Blumenthal, R. Heideman, D. Geuzebroek, A. Leinse, and C. Roelofzen, "Silicon nitride in silicon photonics," *Proc. IEEE*, vol. 106, no. 12, pp. 2209–2231, Dec. 2018, doi: 10.1109/JPROC.2018.2861576.

[11] M. Belt et al., "Sidewall gratings in ultra-low-loss Si_3N_4 planar waveguides," *Opt. Exp.*, vol. 21, no. 1, pp. 1181–1188, Jan. 2013, doi: 10.1364/OE.21.001181.

[12] T. A. Huffman, G. M. Brodnik, C. Pinho, S. Gundavarapu, D. Baney, and D. J. Blumenthal, "Integrated resonators in an ultralow loss Si_3N_4/SiO_2 platform for multifunction applications," *IEEE J. Sel. Top. Quantum Electron.*, vol. 24, no. 4, pp. 1–9, Jul./Aug. 2018, doi: 10.1109/JSTQE.2018.2818459.

[13] D. T. Spencer, J. F. Bauters, M. J. R. Heck, and J. E. Bowers, "Integrated waveguide coupled Si_3N_4 resonators in the ultrahigh-Q regime," *Optica*, vol. 1, no. 3, pp. 153–157, Sep. 2014, doi: 10.1364/OPTICA.1.000153.

[14] M. H. P. Pfeiffer et al., "Photonic Damascene process for integrated high-Q microresonator based nonlinear photonics," *Optica*, vol. 3, no. 1, pp. 20–25, Jan. 2016, doi: 10.1364/OPTICA.3.000020.

[15] G. Z. Mashanovich et al., "Low loss silicon waveguides for the mid-infrared," *Opt. Exp.*, vol. 19, no. 8, pp. 7112–7119, Apr. 2011, doi: 10.1364/OE.19.007112.

[16] R. A. Soref, S. J. Emelett, and W. R. Buchwald, "Silicon waveguided components for the long-wave infrared region," *J. Opt. Pure Appl. Opt.*, vol. 8, no. 10, pp. 840–848, Oct. 2006, doi: 10.1088/1464-4258/8/10/004.

[17] R. E. Camacho-Aguilera et al., "An electrically pumped germanium laser," *Opt. Exp.*, vol. 20, no. 10, pp. 11316–11320, May 2012, doi: 10.1364/OE.20.011316.

[18] J. Liu, X. Sun, R. Camacho-Aguilera, L. C. Kimerling, and J. Michel, "Ge-on-Si laser operating at room temperature," *Opt. Lett.*, vol. 35, pp. 679–681, 2010.

[19] A. W. Fang, H. Park, O. Cohen, R. Jones, M. J. Paniccia, and J. E. Bowers, "Electrically pumped hybrid AlGaInAs-silicon evanescent laser," *Opt. Exp.*, vol. 14, no. 20, pp. 9203–9210, 2006, doi: 10.1364/OE.14.009203.

[20] H. Park, A. W. Fang, S. Kodama, and J. E. Bowers, "Hybrid silicon evanescent laser fabricated with a silicon waveguide and III-V offset quantum wells," *Opt. Exp.*, vol. 13, no. 23, pp. 9460–9464, 2005, doi: 10.1364/OPEX.13.009460.

[21] A. Spott et al., "Interband cascade laser on silicon," *Optica*, vol. 5, no. 8, pp. 996–1005, Aug. 2018, doi: 10.1364/OPTICA.5.000996.

[22] A. Spott et al., "Quantum cascade laser on silicon," *Optica*, vol. 3, no. 5, pp. 545–551, May 2016, doi: 10.1364/OPTICA.3.000545.

[23] D. Liang and J. E. Bowers, "Recent progress in heterogeneous III-V-on-silicon photonic integration," *Light: Adv. Manuf.*, vol. 2, no. 1, pp. 1–25, 2021, doi: 10.37188/lam.2021.005.

[24] J. Justice, C. Bower, M. Meitl, M. B. Mooney, M. A. Gubbins, and B. Corbett, "Wafer-scale integration of group III–V lasers on silicon using transfer printing of epitaxial layers," *Nat. Photon.*, vol. 6, no. 9, pp. 610–614, Sep. 2012, doi: 10.1038/nphoton.2012.204.

[25] R. Loi et al., "Edge-coupling of O-Band InP etched-facet lasers to polymer waveguides on SOI by micro-transfer-printing," *IEEE J. Quantum Electron.*, vol. 56, no. 1, pp. 1–8, Feb. 2020, doi: 10.1109/JQE.2019.2958365.

[26] M. R. Calvo et al., "Mid-infrared laser diodes epitaxially grown on on-axis (001) silicon," *Optica*, vol. 7, no. 4, pp. 263–266, Apr. 2020, doi: 10.1364/OPTICA.388383.

[27] L. Monge-Bartolome et al., "Etched-cavity GaSb laser diodes on a MOVPE GaSb-on-Si template," *Opt. Exp.*, vol. 28, no. 14, pp. 20785–20793, Jul. 2020, doi: 10.1364/OE.397164.

[28] R. M. Joseph and A. Taflove, "FDTD Maxwell's equations models for nonlinear electrodynamics and optics," *IEEE Trans. Antennas Propag.*, vol. 45, no. 3, pp. 364–374, Mar. 1997, doi: 10.1109/8.558652.

[29] K. Yee, "Numerical solution of initial boundary value problems involving Maxwell's equations in isotropic media," *IEEE Trans. Antennas Propag.*, vol. 14, no. 3, pp. 302–307, May 1966, doi: 10.1109/TAP.1966.1138693.

[30] P. Jaturaphagorn, N. Chattham, P. Limsuwan, and P. Chaisakul, "Optimization of end-fire coupling between an LED mid-IR light source and sinx optical waveguides for spectroscopic sensing," *Results Opt.*, vol. 5, Dec. 2021, Art. no. 100174, doi: 10.1016/j.rio.2021.100174.

[31] J. Kischkat et al., "Mid-infrared optical properties of thin films of aluminum oxide, titanium dioxide, silicon dioxide, aluminum nitride, and silicon nitride," *Appl. Opt.*, vol. 51, no. 28, pp. 6789–6798, Oct. 2012, doi: 10.1364/AO.51.006789.

[32] L. G. Aio, A. M. Efimov, and V. F. Kokorina, "Refractive index of chalcogenide glasses over a wide range of compositions," *J. Non-Cryst. Solids*, vol. 27, no. 3, pp. 299–307, Mar. 1978, doi: 10.1016/0022-3093(78)90015-7.

[33] E. D. Palik, Ed., *Handbook of Optical Constants of Solids. 1, 6. Nachdr*. Boston, MA, USA: Academic Press, 2004.

[34] J. K. S. Poon, L. Zhu, G. A. DeRose, and A. Yariv, "Polymer microring coupled-resonator optical waveguides," *J. Lightw. Technol.*, vol. 24, no. 4, pp. 1843–1849, Apr. 2006, doi: 10.1109/JLT.2006.870971.

[35] H. Ma, A. K.-Y. Jen, and L. R. Dalton, "Polymer-based optical waveguides: Materials, processing, and devices," *Adv. Mater.*, vol. 14, no. 19, pp. 1339–1365, Oct. 2002, doi:10.1002/1521-4095(20021002)14:19<1339::AID-ADMA1339>3.0.CO;2-O.

[36] R. Dangel et al., "Polymer waveguides enabling scalable low-loss adiabatic optical coupling for silicon photonics," *IEEE J. Sel. Top. Quantum Electron.*, vol. 24, no. 4, Jul. 2018, Art. no. 8200211, doi: 10.1109/JSTQE.2018.2812603.

[37] X. Zhang, J. Qiu, J. Zhao, X. Li, and L. Liu, "Complex refractive indices measurements of polymers in infrared bands," *J. Quant. Spectrosc. Radiat. Transf.*, vol. 252, Sep. 2020, Art. no. 107063, doi: 10.1016/j.jqsrt.2020.107063.

[38] S. Dhoore, S. Uvin, D. Van Thourhout, G. Morthier, and G. Roelkens, "Novel adiabatic tapered couplers for active III–V/SOI devices fabricated through transfer printing," *Opt. Exp.*, vol. 24, no. 12, pp. 12976–12990, Jun. 2016, doi: 10.1364/OE.24.012976.

[39] S. McNab, N. Moll, and Y. Vlasov, "Ultra-low loss photonic integrated circuit with membrane-type photonic crystal waveguides," *Opt. Exp.*, vol. 11, no. 22, pp. 2927–2939, Nov. 2003, doi: 10.1364/OE.11.002927.